Geoenvironmental Disasters

RESEARCH

Open Access

Engineering geological characteristics and failure mechanics of Jure rock avalanche, Nepal

Suman Panthee[1], Suman Dulal[1], Vishnu Himanshu Ratnam Pandey[2], Vikas Yadav[2], Prakash Kumar Singh[3] and Ashutosh Kainthola[2*]

Abstract

Introduction The rock avalanches are a frequent and disruptive phenomenon in the Himalayas and other mountain chains. To minimize future losses, it is essential to investigate the engineering geological causative factors and mechanism of these mass wasting events.

Study area The present work is aimed at assessing the failure mechanism of the disastrous 2014 Jure rock avalanche along Araniko Highway, Northern Nepal. The event had blocked the Sunkoshi River and blocked an economically significant route to China.

Geotechnical properties and analysis Initially, rockmass characterization and intact strength attribute were determined for the site to classify the failure zone. The parameters measured and obtained from the field and laboratory were integrated into the analytical models to obtain a conclusive interpretation of the failure mechanism. Structural, kinematic, and key block theory analyses have been carried out for decipher the evolution of the failure zone.

Results and discussion Rock mass was found to be of fair quality, however, the structural instabilities and the presence of water has led to a progressive failure. Movement of the key block and subsequent sliding of wedges and foot failure appears to be a possible failure mechanism.

Conclusion The present research explores the contributory engineering geological aspects of the Jure rock avalanche. The investigation results can be used to tackle similar large scale rock avalanches in similar geological terrains and thus minimizing the losses.

Keywords Nepal, Jure, Landslide, Keyblock theory, Rock avalanche

Introduction

The landslides significantly affect mountainous countries like Nepal, India, Switzerland, Japan, Canada, New Zealand, USA, and China (Lateltin et al. 2005; Yin et al 2009; Evans et al. 2011; Bhandary et al. 2013; Dhungana et al. 2023; Xiao et al. 2023). Prakasam et al. (2021) estimated the damages caused by the Himalayan landslides to cost more than one billion US Dollar in economic terms along with more than 200 deaths every year, accounting for about 30% of the total such worldwide losses. Nepal is a part of the Himalayan region and due to its rugged topography and tectonics (Dhital 2015), the country is

*Correspondence:
Ashutosh Kainthola
ashutoshddnuk@outlook.com
[1] Central Department of Geology, Tribhuvan University, Kathmandu 44618, Nepal
[2] Geo-Engineering and Computing Laboratory, Department of Geology, Banaras Hindu University, Varanasi 221005, India
[3] Department of Earth and Planetary Sciences, University of Allahabad, Prayagraj 211002, India

quite susceptible to slope failures and landslides. Over 12,000 small to large scale slope failures occur each year in the country. On 2nd August 2014, a massive landslide occurred at Jure village in Sindhupalchok district on the border of Mankha and Ramche (Ministry of Irrigation 2014). Approximately 5 million m^3 of massive rock fragments and debris were deposited. The landslide killed 156 people, injured 27, and displaced 436 people. The massive landslide dammed completely the Sunkoshi River forming a lake of about 3 km long and 300–350 m in width. The landslide buried about 1 km of Araniko Highway, a major highway leading to china. Other amenities such as school, hospital, police station, and post-office were severely affected. The dust of the landslide reached up to 600 m in height which covered the Dabi Khola village area.

There are several articles on different aspects of 2014 Jure landslides and careful analysis reveals several important information about the mechanism of failure. Bhandary et al. (2018) employed Spectral Element Method (SEM) for analysing stability of wet and dry slopes along with pseudo-static loading of slopes. They highlighted that the slopes become unstable when the groundwater table reaches the surface and peak ground acceleration values become greater than 0.2 g and in some cases even 0.1 g. Jaboyedoff et al. (2015a, b) utilised digital elevation model (DEM) extracted from Terrestrial Laser Scanner (TLS) and field investigations to characterize Jure landslide. They were able to investigate the rockfall avalanche volume, scar structure and deposits. The rockslide was predominantly restricted to phyllites, quartzites and sandstones. Some ephemeral springs were also observed below the unstable mass. The rockslides developed in presence of complex structures is accompanied by degradation of rock mass which further reactivates large scale instabilities. Shrestha and Nakagawa (2016) suggested that existence of unstable slopes and occurrence of previous landslides are responsible for Jure landslides. They further studied areas of flood inundation caused by formation of landslide dam and this study can also assist in implementing mitigation measures for establishing residential areas. Tien et al. (2021) used laboratory tests and numerical simulation to clarify the failure mechanism of the deep-seated landslide and process of dam formation. They suggested that the major slip movement occurred along the bedding plane faults of weathered phyllites and schist. And, more importantly the sliding mechanisms of upper and lower slopes differed from each other. The critical pore pressure ratio of the upper slope reached 0.22 to 0.26 due to heavy rainfall and initiated the failure while the dynamic loading process by downward movement of upper block caused the failure in lower slope. Yagi et al. (2021) combined DEM and InSAR data to detect ground movement. They suggested that prolonged period of creep movement led to the formation of thick weathered layer at the Jure landslide site.

The large-scale landslides are becoming more frequent and is a major cause of disaster leading to huge economic losses (Zhou et al. 2010). The fragile geology, rugged topography, construction activities, heavy rainfall and existence of fault zones allows the hill slope to develop strain over time ultimately leading to slope failures. The massive volume of detached mass generated due to intermittent small landslides and large-scale landslides leads to the deposition of large number of landslide deposits. A major problem associated with large landslide deposits is chocking/damming of a part or entire river. The associated problem with choking of river is lake outburst, flooding of nearby areas, reactivation of old landslides etc. In this regard, Iqbal et al. (2018) have assessed the stability analysis and failure mechanism of an active landslide in Xiangjiaba Reservoir Area, China using field investigation, field monitoring and laboratory tests. Based on geological field investigations, direct shear tests and limit equilibrium methods, stability analysis of the Zheng-Gang landslide, China was studied (Zhang et al. 2014). Mebrahtu et al. (2022) used both limit equilibrium and finite element method to assess the stability of a deep-seated landslide in Debre Sina area, Ethiopia. There are few aspects common in all these analyses related to large scale failures, i.e., saturation threshold, groundwater condition, long-term creeping behaviour, development of localised slip planes, seismicity. The stability of the deep seated landslides triggered by rainfall has also been assessed by estimating the rainfall threshold (Wei et al. 2019; Arnold 2006; Tiwari et al 2020; Kainthola et al 2021; Pandey et al. 2022).

Back-analysis is the process by which the nature and development of a landslide is measured through a series of deductions (Hencher and Malone 2008). Procedure of back analysis start with understanding the subsurface conditions of landslides, defining representative cross-sections, and failure surfaces etc. Appropriate stability method and software should consider varying the landslide ensuing parameters of the problematic layer to the factor of safety (FoS ~ 1.0). Back analysis involves analytical and numerical methods to analyse the available data and determine the factors that contributed to the occurrence of the landslide. Analytical methods engaged theoretical equations and empirical relationships to calculate the stability of the slope and assess the factors that drive to the landslide (Gutiérrez-Martín et al. 2019). These methods include limit equilibrium analysis, slope stability parameters, and analytical solutions for simplified slope geometries. The stability of the

slope is evaluated by comparing the driving forces with the resisting forces. Similarly, different numerical methods are applied to simulate the behaviour of the slope and asses its stability condition (Griffiths & Lane 2001). These models incorporate the geotechnical properties of the rock mass, boundary & initial conditions. The slopes are subjected to various loading conditions, such as vehicle movement, constructions, rainfall and seismicity forming the critical factors leading to failure. And, estimation of shear strength parameters is a prime issue in landslide management, and inappropriate parameter evaluation often guides to the failure of mitigation strategies (Zuo et al.2022). However, it is difficult to accurately examine these parameters due to the complex geological setting and different failure models. Therefore, back-analysis in problematic landslides can be employed to comprehend the critical attributes more diligently than laboratory testing (Hussain et al. 2010).

Literature has the pertinent collection of massive landslides events recorded in the earth's history (Sartori et al. 2003; Dahal and Hasegawa 2008). The critical factors responsible for such failure and associated mechanisms have been highlighted by numerous workers (Cui et al. 2015; Shrestha and Nakagawa 2016; Liu et al. 2023; Wang et al. 2023; Çelik 2023; Yang et al. 2023). Usually, stability of jointed rock slopes is controlled by their joint persistency, spacing of joint sets, and shear strength of the discontinuity (Panthee et al. 2016). The Vargas rock avalanche (Venezuela) of December 1999 is one of the largest reported landslides in the planet's history killing nearly 30,000 lives and was triggered by a heavy storm owing to 911 mm (35.9 in) of rain in a few days (Wieczorek et al. 2001). Similarly, the Armero Tragedy (November 1985) of Colombia had engulfed 23,000 lives (Lowe et al.1986). A catastrophic failure of Aratozawa (Japan) induced by high magnitude (7.2) seismicity had displaced nearly 67 million m^3 (Miyagi et al. 2011). Further studies delineated this landslide as translational block glide having the failure surface in thin sand strata. In 2011, heavy precipitation in Kii Peninsula (Japan) led to several mass-movement, the mechanism and consequent dam formation process of two such deep-seated failures in Kuridaira and Akatani valleys have been detailed in the work of Tien et al. (2018). Li et al. (2011), highlighted the problem of slope failure at Hsiaolin village (Taiwan), thereafter landslide dam formation and simulated eventual dam breaching. A large-scale failure incident led to the emergence of a 60 m high landslide dam at the bank of Jinsha River (SE Tibetan Plateau) by disposing nearly 4.9×10^7 m^3 of debris materials (Li et al. 2011). Additionally, the buckling of planar blocks under the effect of gravitational force had initiated the failure, as confirmed by fieldwork and theoretical examination. In 2020, the Pettimudi landslide (India), an extreme-rainfall triggered cataclysmic mass-movement that had affected an area of 70,125 m^2 (including tea-plantation) and claimed 66 natives' lives (Achu et al. 2021). A prolonged precipitation event triggered the deadly Malpa rockfall-debris flow (1998) in the Indian Himalaya that invited 221 fatalities, and partially dammed the Kali River by pouring nearly 1 million m^3 (Paul et al. 2000).

The previous investigation on Jure landslide lacks an in depth engineering characterization of material and detailed analysis of the mechanism of failure that led to this catastrophic event. Therefore, the present study is aimed at investigating the causes and failure mechanism of the Jure rock avalanche. A detailed visualization of the geomorphic scenario and engineering geological mapping of the research area is essential to comprehend the landslide occurrence. The rockmass characterisation and intact strength attributes determination will enable numerical simulation of the failure zone. Moreover, back analysis of the landslide by analytical and numerical methods will advance the landslide knowledge. The parameters measured and obtained from the field and laboratory were integrated in the analytical and numerical models to obtain the conclusive interpretation. RS^2 software was used for finite element numerical modelling. The results computed by various methods complementary to each other were then integrated to know the evolution history and mechanism of slope failure.

Study area

The study area is about 83.5 km northeast of Kathmandu at the right bank of the Sunkoshi River, near Barhabise Bazar, Sindhupalchok district, Central Nepal (Fig. 1). The study area is easily accessible by the Araniko Highway and is drained mainly by the tributaries of the Sunkoshi River flowing in NE to SW direction. The climate is subtropical, temperate, and alpine. The average rainfall is 3604.3 mm, of which 80% falls in the monsoon season. A temperature ranges of about 30°–32 °C can be expected during summer, and it varies from about 6°–8 °C during winter months. Geologically, the Nepal Himalaya is divided into five major geological zones: Terai, Sub-Himalaya (Siwaliks), Lesser Himalaya, Higher Himalaya, and Tibetan-Tethys Himalaya (Gansser 1964; Upreti 1999). And, the basic framework of the Himalayas is controlled by three significant thrusts, Main Central Thrust (MCT), Main Boundary Thrust (MBT), and Himalayan Frontal Fault System (HFFS) that dip north and extend east–west throughout the country (Upreti 1999). These three thrusts are considered to come together in a low angle decollement known as the Main Himalayan Thrust (MHT) to the north, deep below the Himalaya.

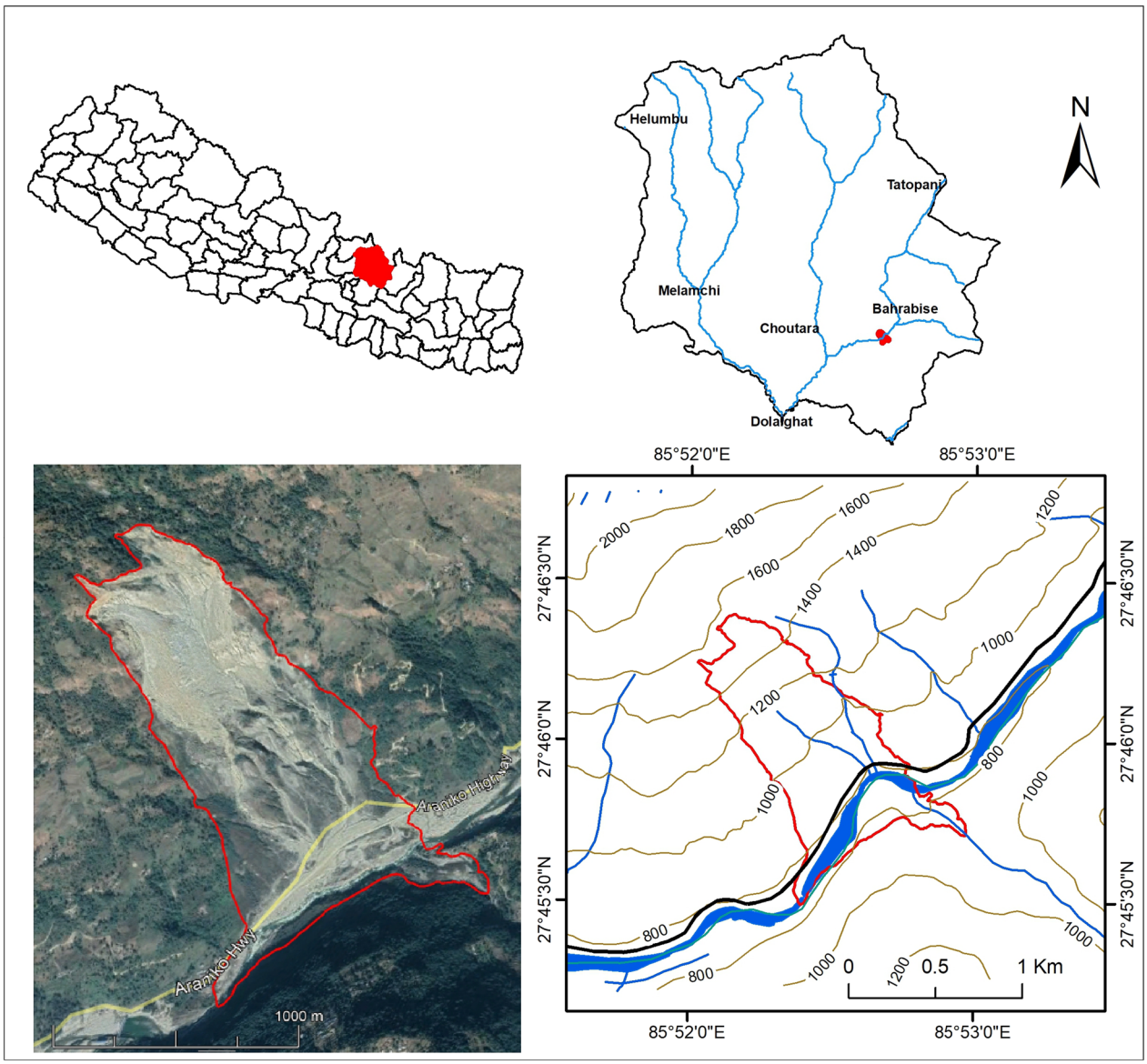

Fig. 1 Geospatial and geomorphological aspects of the Jure landslide

The study area lies within the Kuncha Formation of Lesser Himalaya (Central Nepal) comprising meta-sandstone, chloritic schist and pelitic schist (Fig. 2). Kuncha formation ranges from the Gandaki Region to the Bagmati–Gosainkund Region. In the Gandaki region, the inner zone of Gorkha is made essentially of the Kuncha formation. In this region, the Kuncha formation appears immensely thick, monotonous succession of dark grey, green-grey, bluish-grey phyllite, phyllitic metasandstone, gritty phyllite, and quartzite. Dhading Dolomite forms hills and ridges around Dhading and varies in thickness from 500 to 1000 m. Metasandstone and phyllite is the main lithology of this formation and belongs to the Mesoproterozoic Era. Nourpul Formation begins with a few centimetres to decimetre green-grey and purple phyllites. And, marble and schist are the main lithologies of this formation with approximately 800 m thickness formed in Mesoproterozoic. Furthermore, Fagfog formation consists of Fagfog quartzite of Paleoproterozoic Era as their main lithology having a thickness of 400 m. This quartzite shows graded bedding, cross-lamination, and spectacular wave and current ripple marks. Fagfog Formation abruptly over the Kuncha Formation and it consists of fine to coarse grained light grey, pale yellow, and white quartz arenites with thin grey-green phyllite alterations or partings. Auden (1937) established a relationship

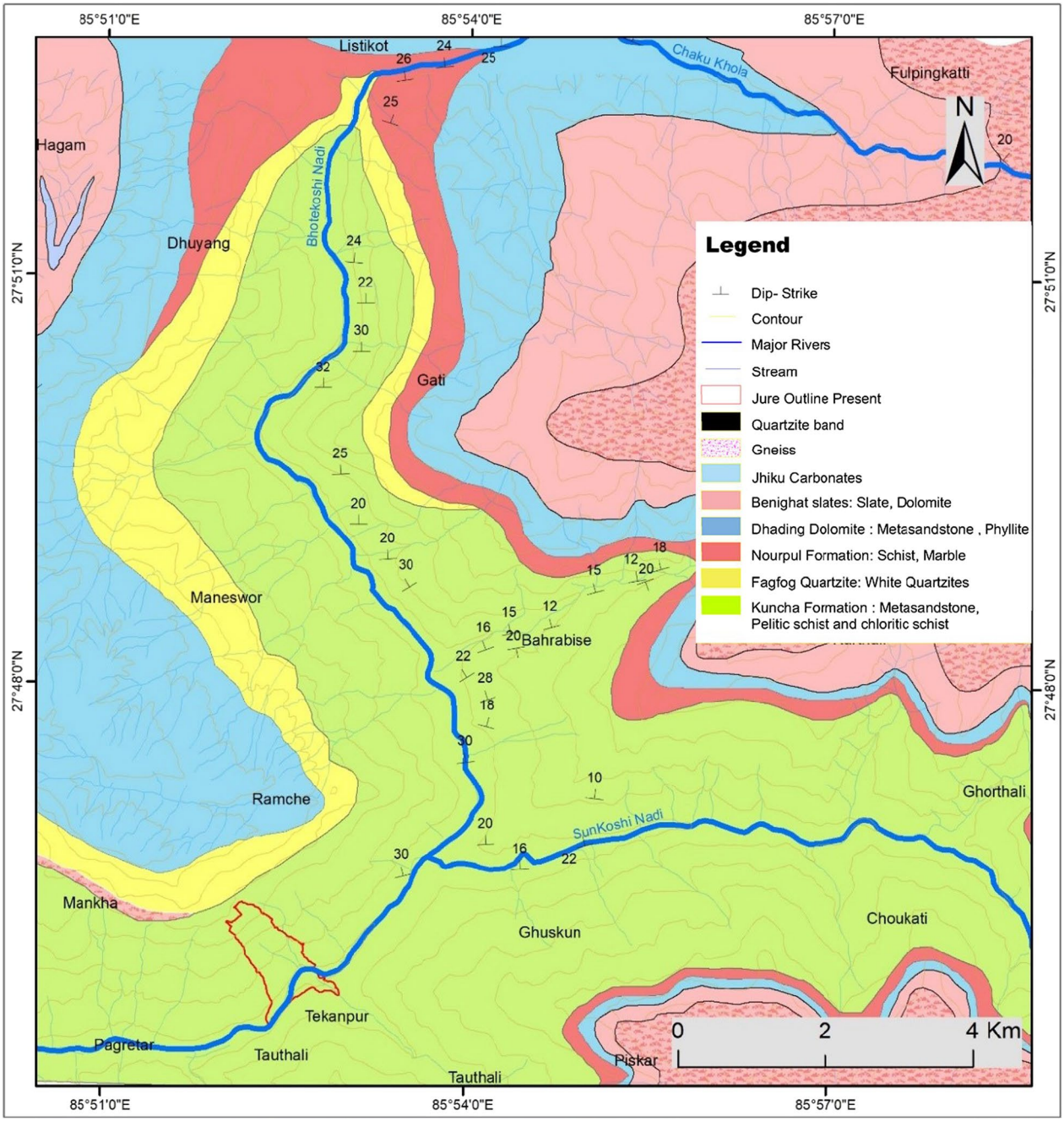

Fig. 2 Geological map of study area (modified after Budhathoki (2016))

between the Benighat slates and the Jhiku formation of Udaipur in east Nepal with the Blaini and Krol series. It contains very thinly cleaved varieties. Slate, argillaceous dolomite is the main lithology of this formation and it is referred to as Benighat slates. The age of the Benighat slates is Mesoproterozoic. Jhiku carbonate bed lies with Benighat slates. There are some specific zones rich in carbonates classified as calcareous beds or Jhiku carbonates (Stöcklin and Bhattarai 1977). The major anticline axial trace is horizontal and passes along the Sunkoshi River trending NE-SW direction. The foliation plane of limbs dips gently in two different directions (Budhathoki 2016).

Jaboyedoff et al. (2015a, b) characterized the Jure avalanche and analyzed the rock fall avalanche volume, scar structure, and deposits. The estimated rockslide volume was approximated to be 5 million m^3. In addition, some

ephemeral springs seemed to develop below the unstable mass. The rockslide generated the rock avalanche. Rock avalanches are a type of mass movement entailing rapid downward motion of fragmented rocks from a large rock mass mounted over the steep slopes, quite common in this region (Shrestha and Nakagawa 2016; Tien et al 2021; Yagi et al 2021). The landslide activities in Nepal can be attributed to severe climatic, topographic, and geological circumstances (Ministry of Irrigation 2014). The issue has been further aggravated due to Nepal's active tectonics, steep topography, and anthropogenic activities (Bhandary et al. 2018). Arnold (2006) classified the country under moderate to high landslide hazard zone.

Geotechnical properties and analysis

Rock mass properties

The mapping of fractures in the Jure landslide zone started in 1958 during the construction of Araniko highway. In 1967, 1971, and 1975 landslides were repeatedly observed just below the crown. In 1983, a landslide occurred on the crown, however the toe remained safe. After 1989, landslides activated and regenerated below crown to mid part. The GoogleEarth images since 2012 indicate an increasing rock fall and scarp development activity of the landslide. There was a smaller slide in 2013 at the upper cliff. The slide reactivated suddenly on 2 August 2014 causing a huge collapse. Figure 3 shows the pre and post landslide features of the Jure landslide.

The engineering geological mapping was done to assess different parts of the landslide (Fig. 4). Numerous quartz veins are visible, and most are aligned parallel to the foliation. The foliation of the rocks gently dips about 10°-25° toward NW. The other two major joints are almost vertical, joint dipping 70°-80° towards East (J_{S1}), from which most of the water is flowing down and joint dipping 80°–85° towards southwest (J_{S2}). The kinematic analysis shows that failure in the lower cliff is unlikely. On the upper cliff, some wedges are formed on the left flank of landslide, implying possible wedge failure and on other parts wedges formed by intersection of joint planes J_{S1} and J_{S2} were observed which were stable without any external forces. The Jure landslide is a form of mass wasting that includes a wide range of ground movements such as rock falls, deep failure of slopes, and shallow debris flows. Although, the action of gravity is the primary driving force for a landslide to occur, there are other contributing factors affecting the original slope stability. In this landslide,

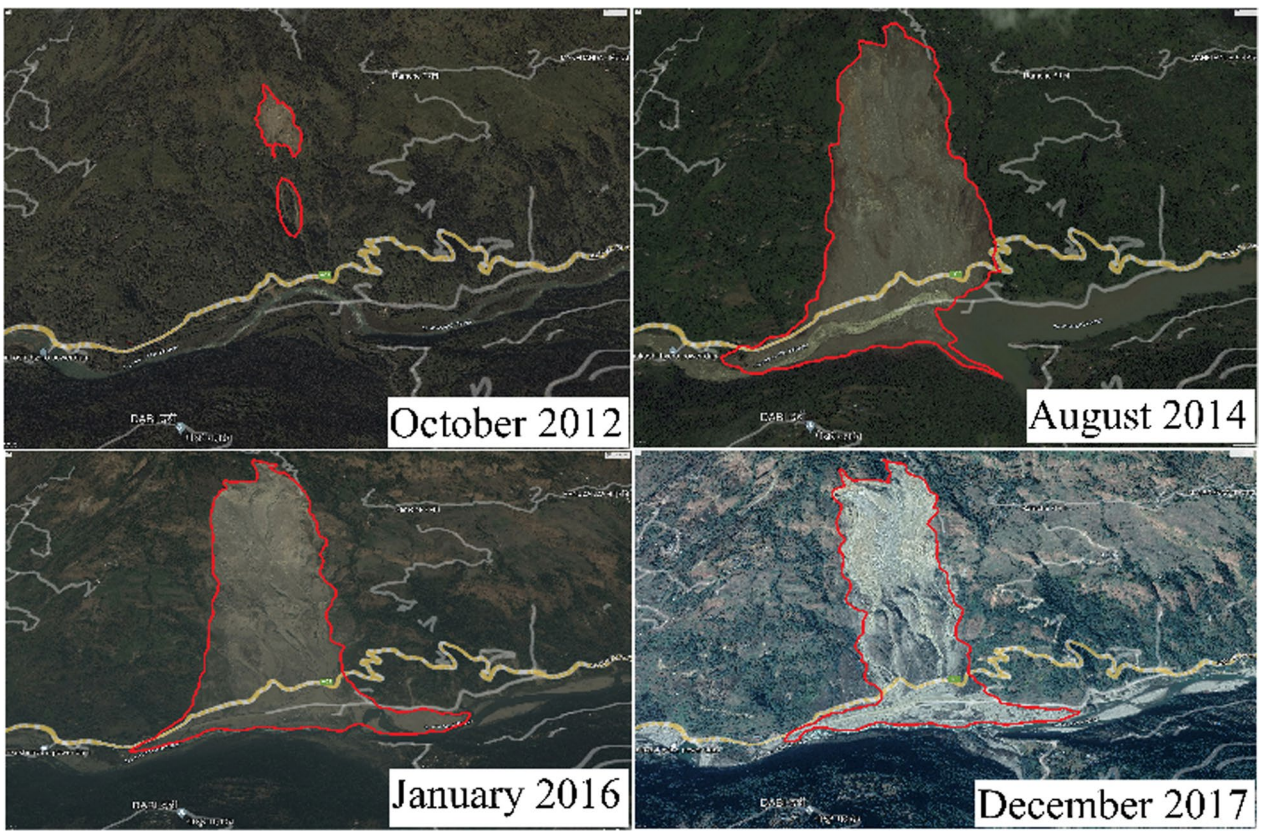

Fig. 3 Google earth images of 2012, 2014, 2016, and 2017 of the study area

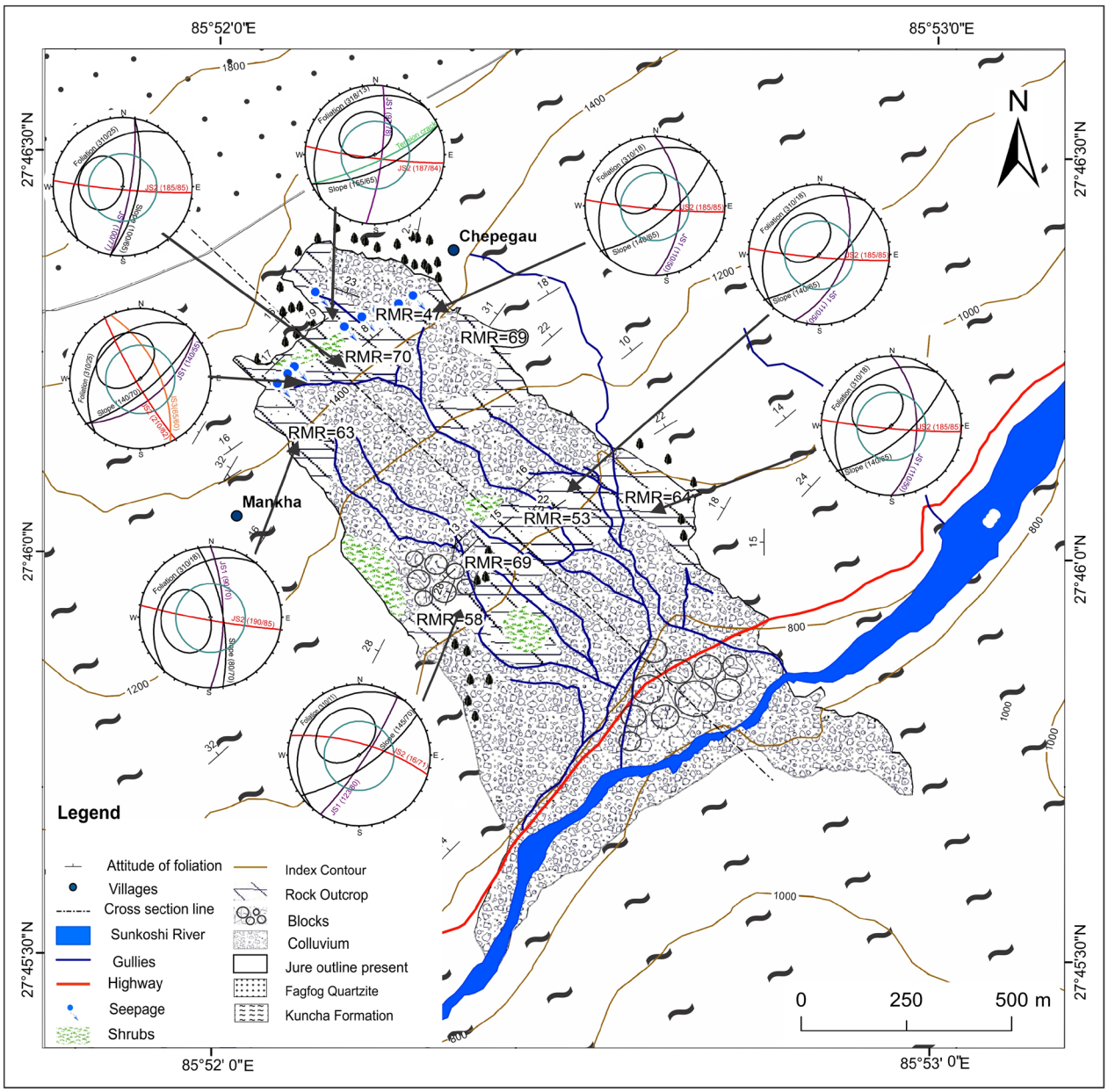

Fig. 4 Engineering Geological map of study area

the sliding surface is mostly deep below the maximum rooting depth of trees typically to depths greater than ten meters. The concave scarps at the top and steep areas at the toe can be visually identified from landslides. There are still large cracks present in the upper cliff from where the spring water is coming out (Fig. 5). Moreover, the cross-sectional view of the Jure landslide can be inferred through Fig. 6.

The Jure landslide is geomorphologically divided into six zones, based on the parameters like slope angle, rock formation, and condition of spring source as shown in (Fig. 7).

The crown is full of cracks, from where the spring water is discharging (zone 1). At this section, the slope is found to be 70°-80° with concavity throughout the slip surface. The slippage initiated from upper cliff (zone 2). At this section, the slope is found to be 65°-70° with concavity throughout the slip surface. This segment consists of highly weathered rocks. The exposed scar looks brownish in colour. Zone 3 comprises huge boulders and rock

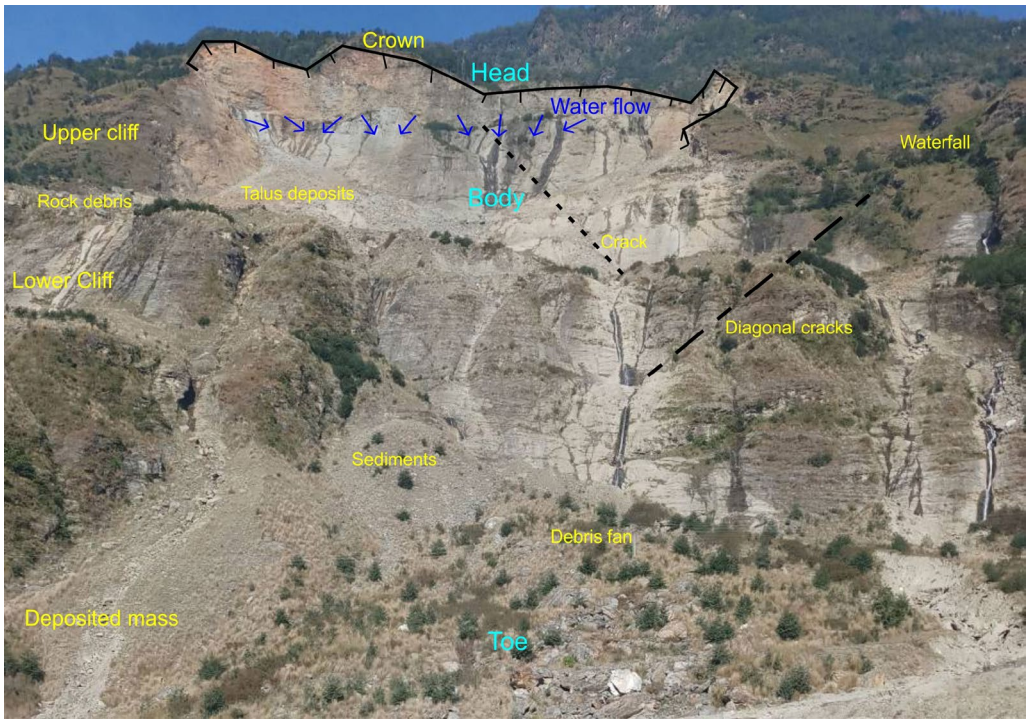

Fig. 5 Jure rock avalanche showing different parts (view to N)

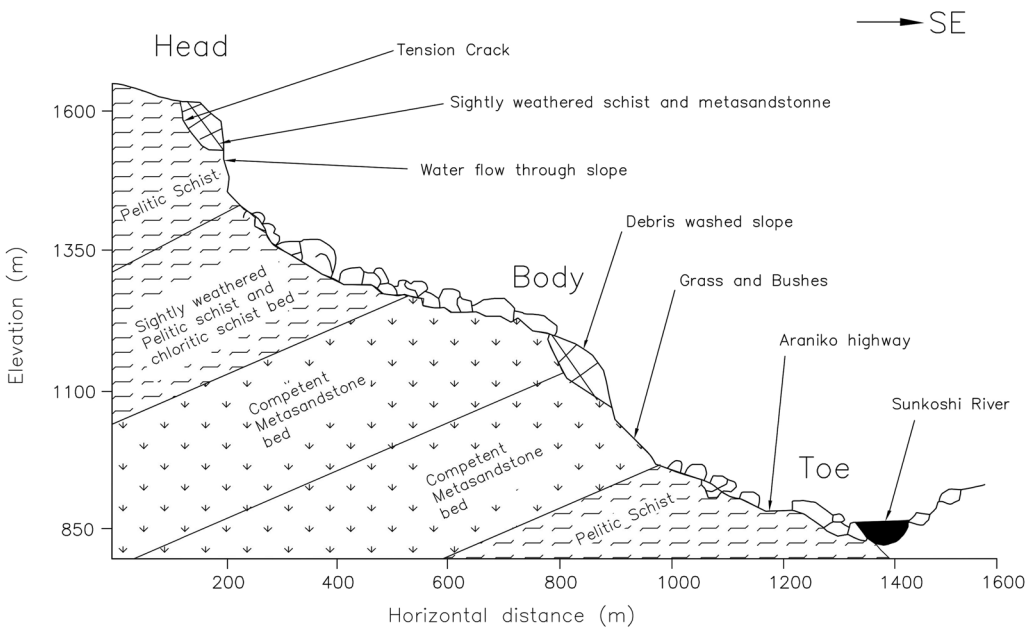

Fig. 6 Cross section of Jure landslide showing various landslide parts

fragments covering the flat land between the Lower and Upper cliff. This section of landslide consists of an abundance of debris material. The slope ranges from 30°-45°. The spring source flowing downwards from top of the slope follows this section along the surface. Zone 4 of the landslide is the remains of the previous slope signifying the low potentiality of failure and the slope of this section is 55°-65°. This section primarily consists of highly

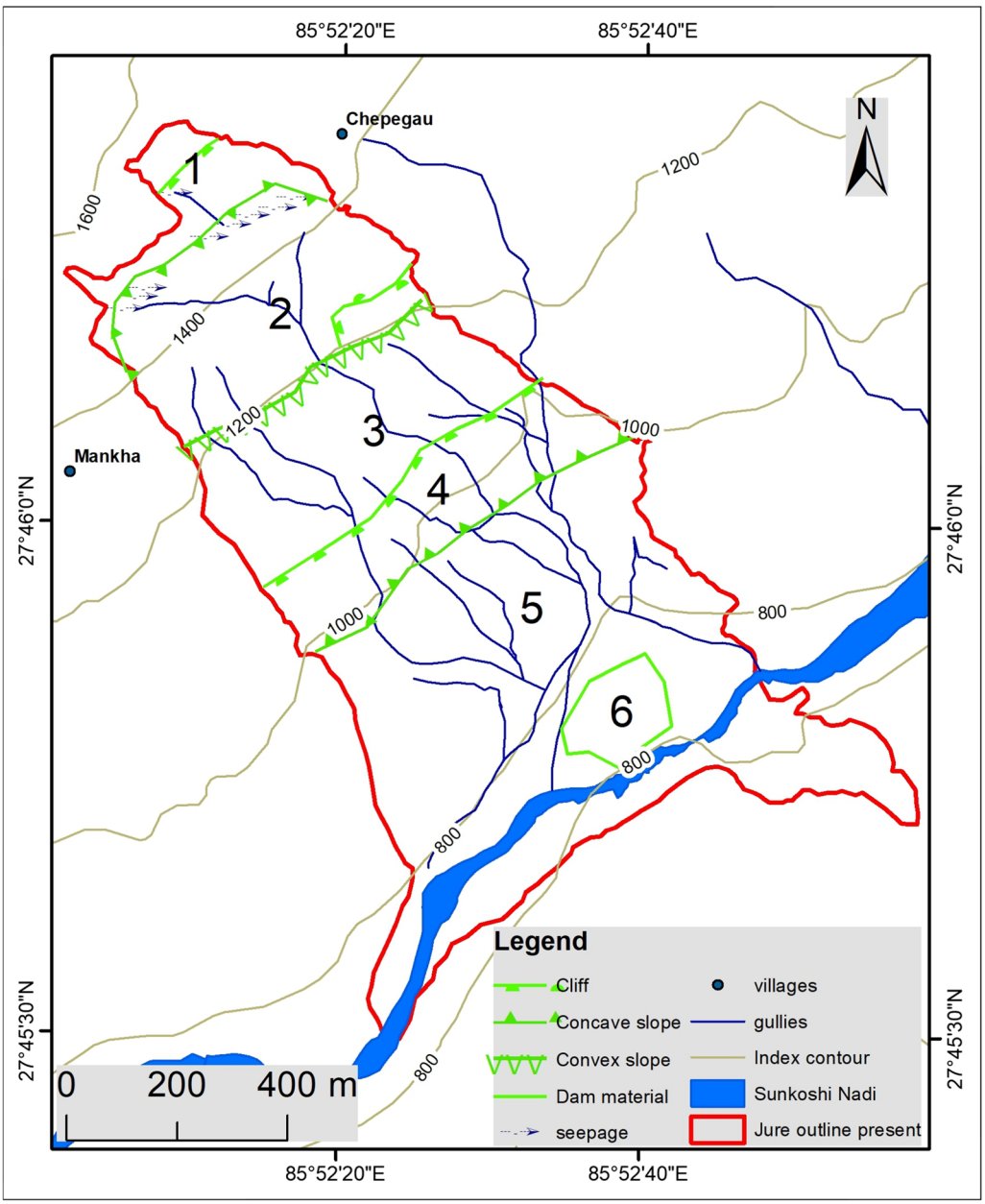

Fig. 7 Geomorphological map of Jure landslide showing various failure zones

fractured rocks at the surface. The spring source that has been disappeared in, again appears at this section forming the distinct gullies. Zone 5 can be described as toe or debris fan deposit area of the landslide comprising colluvium. Zone 6 is the accumulation zone of failed mass that consists of large boulders dispersed in different sections throughout the landslide areas at toe.

An exhaustive field investigation was carried out to record the data pertaining to rock type, discontinuity characteristics, and rock mass. The joint volume (J_v) was calculated from the same data which was further used to calculate RQD and rock mass rating (Table 1).

The discontinuity persistence, aperture, roughness, infilling, and weathering along with hydrological conditions were assessed to calculate the rock mass class (Bieniawski 1973). Most of the rock mass fall in the fair to good rock class.

Table 1 Attributes of rockmass recorded during field investigation

Location		Lithology	RQD	UCS (MPa)	RMR	Rock class
Easting (E)	Northing (N)					
389098	3072308	Metasandstone	58	154	64	Good
389096	3072318	Pelitic Schist	49	53	54	Fair
389082	3072335	Pelitic Schist	10	60	45	Fair
389064	3072362	Metasandstone	81	160	69	Good
389057	3072481	Pelitic Schist	26	56	51	Fair
389078	3072496	Chloritic Schist	10	56	47	Fair
389508	3072621	Metasandstone	69	156	63	Good
388446	3073134	Pelitic Schist	58	45	63	Good
388315	3072887	Metasandstone	68	148	68	Good
388305	3072874	Pelitic Schist	80	56	59	Fair
388565	3072782	Chloritic Schist	56	56	63	Good
388675	3072964	Metasandstone	78	156	70	Good
388714	3073081	Chloritic Schist	35	45	47	Fair
388923	3073019	Pelitic Schist	48	53	69	Good
389285	3072653	Metasandstone	74	164	64	Good
389055	3072610	Metasandstone	65	156	53	Fair
388982	3072479	Pelitic Schist	66	60	69	Good
388808	3072377	Chloritic Schist	49	58	58	Fair

Table 2 Mean Geotechnical properties of rocks from Jure rock avalanche (Bray 2016)

Parameters	Meta-sandstone	Pelitic Schist
Unit weight	26.3 kN/m^3	26.5 kN/m^3
Uniaxial Compressive Strength	156 MPa	56 MPa
Tensile Strength	15 MPa	4 MPa
Friction angle (Peak)	47.4°	17.2°
Friction angle (Residual)	38.6°	17.1°
Apparent (Cohesion-peak)	3.2 MPa	4.7 MPa
Apparent (Cohesion-residual)	1.6 MPa	9.7 MPa
Young's modulus	16–29 GPa	3–4 GPa
Poisson's ratio	0.23	0.3

Intact rock properties

The rock samples were tested in the laboratory of University of Leeds, United Kingdom to determine strength parameters of intact rock (Bray 2016). The samples taken were mainly blocks from the landslide debris. Only samples with no obvious discontinuities were chosen for testing, however during the landslide it is likely that some internal fractures may have formed, reducing the strength of these fallen blocks. The nine parameters of intact rock were determined in the laboratory (Table 2).

Kinematic analysis

The three major discontinuities including the foliation plane were identified at the rock avalanche site. There are numerous tension cracks developed above the crown of the landslide, dipping parallel to the hillslope. The geometry of tension cracks is also included in the analysis. According to the locals, there were large tension cracks above the head from where stream water was flowing down. The tension cracks were nearly parallel 155° with near vertical inclination.

Most tension cracks parallel to slope had slightly greater inclination than the slope, denoting minimal chances (~6%) of plane failure (Fig. 8). Moreover, no wedge instability can be located considering mean orientation of major discontinuities from the upper cliff. However, two very gentle wedges formed by the intersection of foliation with J_{S2} and J_{S1} at the western and northern parts of the stereoplot (Fig. 8). Another three very steep (nearly vertical) wedges formed by J_{S1} and J_{S2}, tension crack and J_{S1}, and tension crack and J_{S2} are not daylighted. Additionally, there are no such discontinuities which may be responsible for the toppling failure (Fig. 8). This indicates none of the simple failure modes appear to be feasible. So, the water flowing from the tension crack may have ultimately appended the water pressure along joints, eventually lifting or pushing the wedges. This gives rise to the possibility of generation of newer fracture planes enabling sliding of the slope mass.

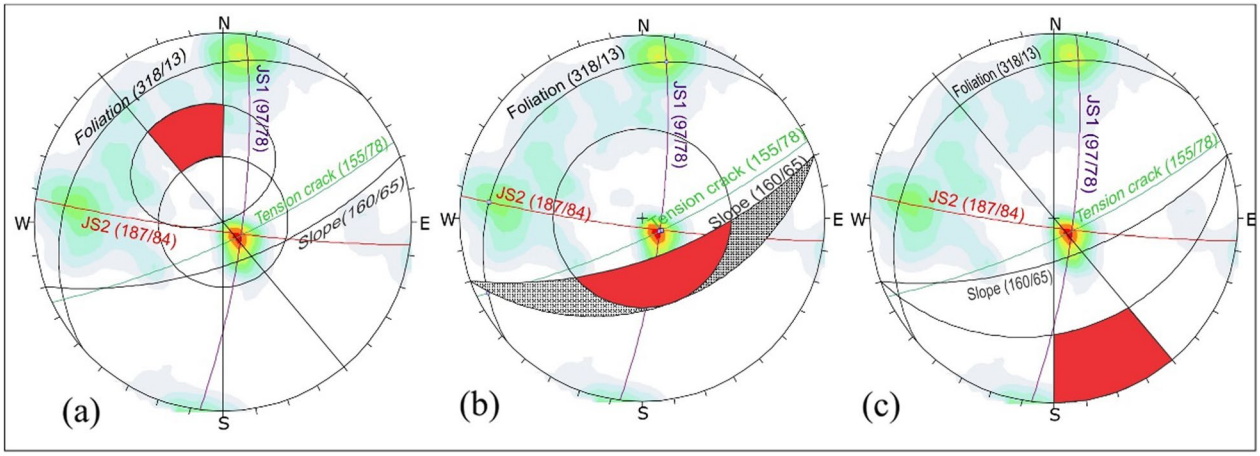

Fig. 8 Kinematics analysis for failures, **a** planar failure, **b** wedge failure, **c** toppling failure

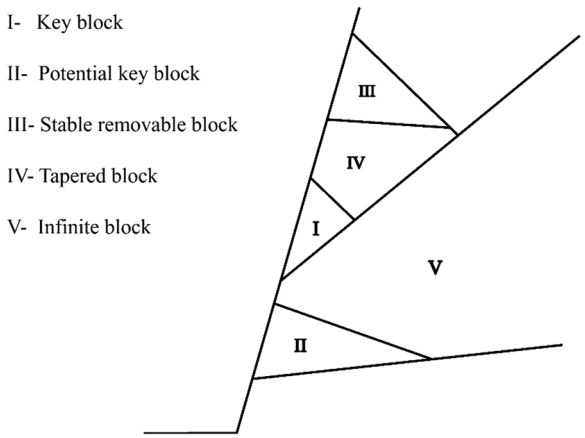

Fig. 9 Key block theory classification of rock blocks (Kulatilake et al. 2011)

Block theory analysis

The block theory considers the geometry of the discontinuities and the slope orientation, in a similar manner to the kinematic analysis. In addition, it determines the "finiteness" of blocks bounded by several discontinuities and free surface along with their removability. According to the key block theory, a rock slope is stable if the weight of the rock above the key block is balanced by the friction and shear resistance of the key block against the rock below it (Fig. 9). If the weight of the rock above the key block exceeds the resistance of the key block, the slope becomes unstable and may fail.

One of the main advantages of the key block theory is that it provides a simple and intuitive way to understand the mechanics of rock slope failure. It also allows engineers to identify the key blocks in a rock slope and determine the forces acting on them, which can be used to design mitigation measures to improve the stability of the slope. However, the key block theory has some limitations, as it does not consider the effect of rock jointing and other factors that can affect the stability of a rock slope. Despite these limitations, the key block theory remains a valuable tool for analysing and predicting the stability of rock slopes. The present work delves into key block analysis over the dataset outlined in Table 3. The Key block theory was performed using stereographic projection of joint planes on the upper hemisphere (Fig. 10).

The stereographic projection delineates 14 joint pyramids, representing the 14 different types of block formation from the intersection of discontinuities (Table 4). The factor of safety of such formed blocks in relation to free surface was determined. Out of 14 various shaped

Table 3 The mean orientation and properties of major discontinuities

Joint set	Dip Direction	Dip Amount	Spacing	Aperture	Infilling	JRC	JCS
Foliation	318	13	1 m	> 200 mm	Quartz	2–4	40
J_{s1}	097	78	10 m	< 200 mm	Platy	4–6	90
J_{s2}	187	84	15 m	Tight to open	Quartz	6–8	90
Tension Crack	155	78					
Hill Slope	160	65					

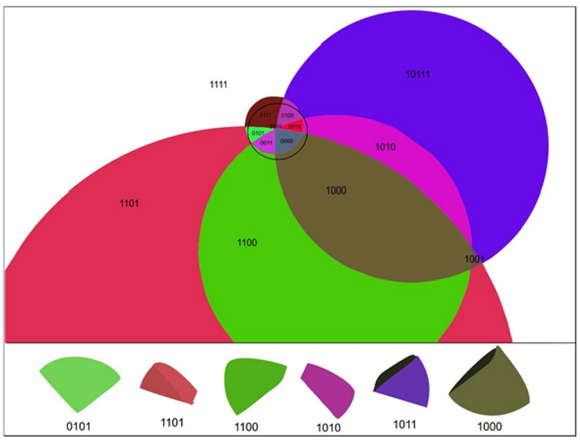

Fig. 10 Joint pyramids and critical block shapes analysed from block theory analysis

and sized key blocks types, 6 were finite and removable (i.e., Joint Planes: 1000, 1100, 1010, 0101, 1101, and 1011) with FoS less than 1. A slight movement in these blocks by any external pressure and loading can cause these blocks to move. Consequently, the overlying blocks become free to move causing the failure to progressively become larger in a chainlike series.

Plane failure analysis

The tension crack in relation to slope was further examined to determine susceptibility of planar failure along the crack. The role of pore water pressure along open joints/ planes were also investigated. The critical tension crack position and its depth was determined based on trace observed at the avalanche. The height of water in the tension crack was gradually raised by hit and trial of 500 different combinations in order to cause failure on the sliding planes. Simultaneously, their corresponding factor of safety was determined. Afterwards, computer simulations for plane failure analysis were performed using the most critical conditions from parameters, as obtained in back analysis (Fig. 11). The calculation shows the slope was marginally stable in absence of any external forces. The dip of the sliding plane, upslope dip amount, and face dip amount were 48°, 32°, and 65° respectively as input parameters in back analysis of the Jure slope. Additionally, critical tension crack depth, position for tension crack, critical slide plane inclination was fed as 41.86 m, 33.60 m, and 51.50°, respectively. The factor of safety of the slope without water and with water in tension crack is calculated to be 1.7 and 0.59, respectively.

The spring water infiltrates through the tension cracks and J_{S1} leading to the alteration and degradation of rock mass. The process also increases the pore water pressure in the tension crack at the slope's toe. The water pressure in these cracks allowed the block movement by the forces developed on the joint surfaces resulting in tilting of the blocks from the toe and ultimately slope failure. The sensitivity analysis indicates the variation in FoS with change in slope parameters such as slope angle, height, or water percent filled in tension cracks (Fig. 12). The back-analysis using hit and trial approach gave a perfect match with the result obtained from computation in RocPlane software (RocScience Inc.). Furthermore, the sensitivity analysis also fits the real ground condition (Fig. 12).

Table 4 Block classification and corresponding FoS

S. No.	Colour	Planes	Mode	Safety coefficient	Sliding Direction
01		0000	Stable	01.00	(0.000, 0.000, 0.000)
02		1000	Key	00.21	(0.191, -0.139, 0.972)
03		0100	Potential	09.90	(-0.899, -0.434, 0.97)
04		1100	Key	00.16	(0.0879, -0.188, 0.97)
05		0010	Stable	01.00	(0.000, 0.000, 0.000)
06		1010	Key	00.54	(0.212, -0.129, -0.969)
07		0110	Stable	01.00	(0.000, 0.000, 0.000)
08		1001	Stable	05.21	(0.193, -0.172, -0.973)
09		0101	Key	00.24	(-0.980, -0.102, -0.169)
10		1101	Key	00.08	(-0.0127, -0.104, -0.99)
11		0011	Potential	06.15	(0.151, 0.978, -0.144)
12		1011	Key	00.16	(0.206, -0.0253, -0.97)
13		0111	Potential	30.38	(-0.652, 0.724, -0.225)
14		1111	Stable	01.00	(0.000, 0.000, -1.000)

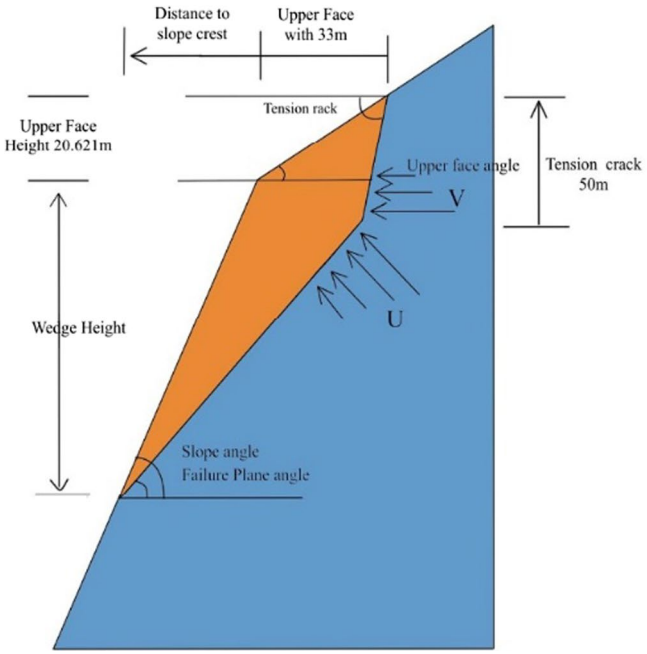

Factor of Safety	0.59
Driving Force	180.3 t/m
Resisting Force	107.2 t/m
Wedge Height	161.8 t/m
Wedge volume	5781.2 t/m
Shear Strength	106.8 t/m
Normal Force	4.3 t/m
Plane waviness	5°
Water Force on Tension crack	120.02 t/m

Fig. 11 Planar wedge stability analysis of Jure slide

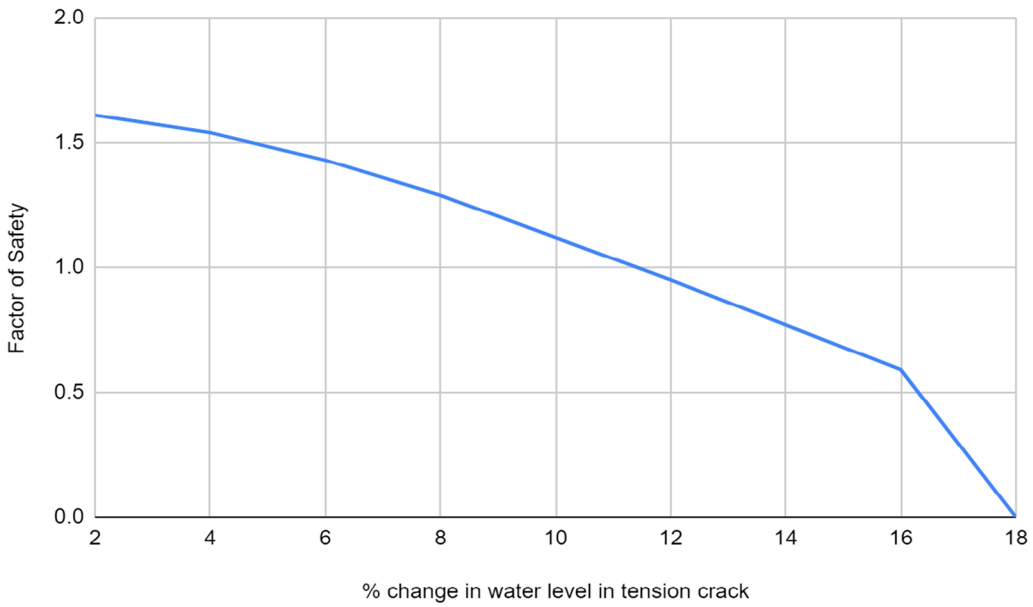

Fig. 12 Sensitivity analysis for various slope parameters for planar failure

Wedge analysis

The study further investigates wedge failures, as per structural discontinuities and examines wedge surfaces in rock slopes. In this analysis, the tension crack was added to form the rear release surface. The kinematic approach using the discontinuity sets indicated stable geometries of wedge formed by J_1 and J_2. As the hillslope direction varies throughout the slope, various other valid directions of hillslopes are tested to obtain wedge blocks of different shape and size. All the possible combinations of two discontinuities and the slope surface that form a valid wedge were analysed (Fig. 13). The wedges are found to have a maximum weight of 155 tons, and with addition of water force in the most critical wedge formed by J_1 and J_2,

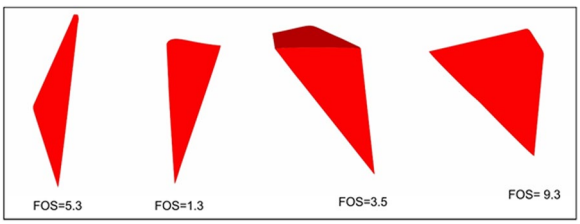

Fig. 13 Various shaped and sized blocks formed by wedges in Jure

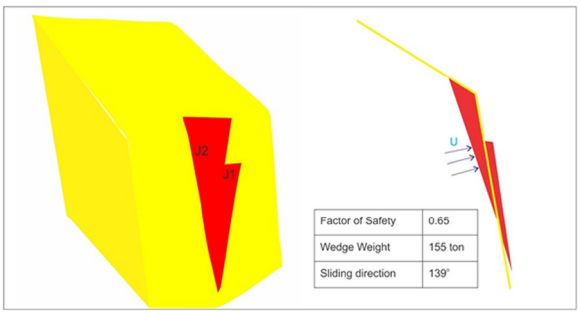

Fig. 14 Wedge stability analysis for most critical wedges

the FoS is found to be 0.65 (Fig. 14). The water infiltrating through the joint intersection increases the water pressure in the walls of the joint that pushes the wedge. The development of pore water pressure at the base of the wedge caused the toe of the block to tilt and decrease in plunge which subsequently failed by sliding along the line of intersection, trending 139°.

Results and discussion

The primary objective of the study is to undertake geo-engineering investigation and to interpret the failure mechanism of the landslide. The variation in rock mass classes is due to the differing rock quality designation (RQD), spacing of discontinuity, condition of discontinuities, and ground water condition (Bieniawski 1989). The intact physico-mechanical attributes and discontinuities' shear strength variables were discerned through laboratory and in-situ testing. The Pelitic schist was found softer having fine grained minerals and mica dominating with smooth surface indicating low Rock Mass Rating (RMR = 50) whereas metasandstone has high RMR value (RMR = 64).

The satellite images since 2012 indicate an increasing rock fall and scarp development activity at the incident site (Fig. 3). However, it was difficult to assume the occurrence of such a catastrophic mishap. The records show that no seismic events were recorded prior to the failure, however, rainfall of more than 70 mm/day was recorded two days before the mishap. The natives have noticed muddy water flowing through the landslide mass in the last 3 days before the event. The high groundwater table weakened the critical rock bridges, causing explosion-like fracturing of rocks and the expulsion of the key block, followed by sliding and foot failure of the other rock blocks. The analysis showed that shifting of water level in joints and tension cracks can cause abnormal failure of slope. The rainfall, two days prior to the event, led to increase in water level and is the main reason behind the failure.

The interpretation of the evolution of the 2014 Jure rock avalanche can be seen in Fig. 15. The surface water infiltrates through tension cracks and joint networks over a period of time causing widening of joint apertures owing to freeze–thaw action and ultimately weakening the rock mass through physical disintegration process. The heavy rainfall (70 mm/day), prior to the event, influenced the pore water pressure in impervious and porous pelitic schist rockmass obstructing the flow by infilling materials in tension crack and some of the discontinuities. The impervious boundary allowed high water pressure to be concentrated on the walls of tension cracks and the toe of the blocks at the base of the upper cliff (Fig. 15a). And, this increase in pore water pressure along the structural discontinuities had significantly lowered the shear strength attributes along joints' surfaces and eventual decrease in factor of safety (FoS) value. Also, the hydrostatic pressure developed in the rockmass owing to heavy rainfall exceeded the static friction threshold of rock blocks and wedges. And, as the concentration is reached maximum around key blocks, the blocks in front are pushed forward. The tilting and pushing of key blocks by water pressure from the joint networks and base of blocks caused the blocks of schist (the key-block) to bulge out which ultimately was thrown outward along the gentle foliation plane (Fig. 15b). With the support removed below, the above hanging rocks became unstable as discussed above in the key-block theory section. And, around 80 m high rock cliff collapsed from the upper cliff on removal of key block support from below (Fig. 15c–f) and the debris moved downhill triggering the mass movement by washout of bedrock in the lower cliff. At this stage, the debris lost its momentum reaching the narrow valley floor where it buried the Araniko Highway, as well as some houses. Finally, the debris and blocks from the avalanche dammed the Sunkoshi River forming a landslide dam. Furthermore, the material forming the crown of avalanche became unstable, when the rock mass constituting the upper cliff was moved downhill. The movement propagates towards the crown after the main failure event happened (Fig. 15d). It can be observed that streams flowing downward above the crown and landslide mass has infiltrated through open joints. There is

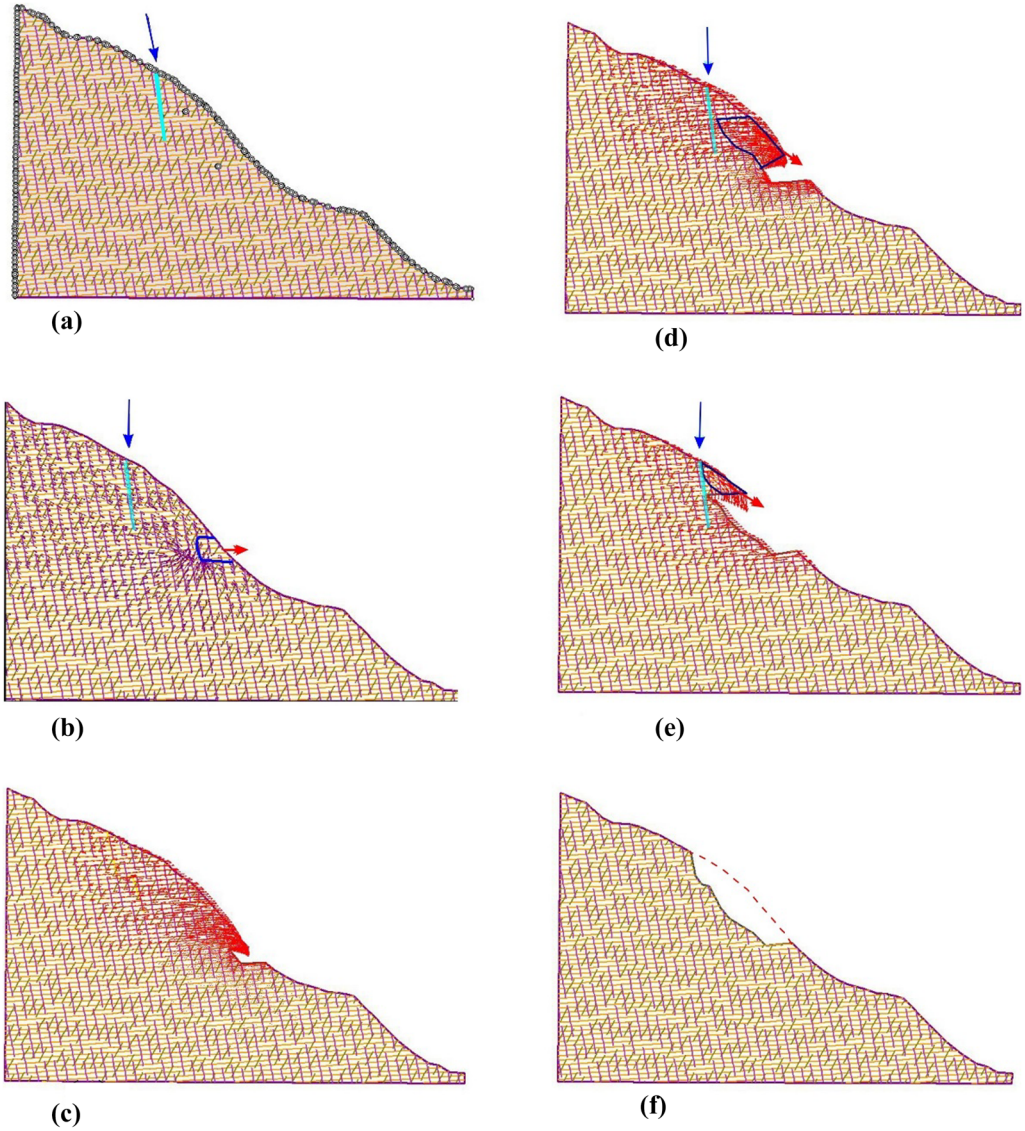

Fig. 15 Evolution and failure mechanism of Jure rock avalanche

still a large crack present in the upper cliff from where the spring water is coming out. The tilting of trees in different directions can be observed above the crown. The reactivation of slope during rainfall and in dry season occurs by smaller failures on crown area.

The Jure failure appears like a translational rockslide (Varnes 1978), since translational movement of rock occurred along a more-or-less planar or gently undulating surface (Dhital 2014). Also, it looks like a block failure where key blocks formed by intersection of discontinuities were displaced due to increase of water pressure, and subsequently caused the larger failure of overlying mass along tension crack and discontinuities. Therefore, the Jure rock failures seem a complex and a special type of landslide. A very large quantity of saturated substrate material represents an unusual type of landslide, termed as rock avalanche. Many rock avalanches can thus be seen as end members of a continuum of phenomena involving rock failure followed by interaction with saturated substrate (Hungr and Evans 2004). Based on the nature of the failure mechanism and debris movement, the present case can be a rock avalanche.

In Jure, the rock fragments were dropped from about 800 m height to the base of the landslide, so the speed could be approximately 60–70 m/s (Dhital 2014). The rock avalanche is an extremely rapid, massive, flow-like motion of fragmented rock from a large rock slide and rock fall (Hungr et al. 2001). Again, based on the speed

of material it should be classified as a rock avalanche. The Jure failure has a volume of 5.05 million m^3 and based on volumetric nomenclature a rockfall having a volume of more than 1 million m^3 will be classified as a rock avalanche. Generally, these slope failures are complex and will take place in two stages. Dikau et al. (1996) describes the mechanical analysis of a rock avalanche as "a fall or slide of a rock body which during movement progressively loses its cohesion by turning into dry debris and thus continues its advancement as a debris avalanche". The debris at the base of the slope at Jure is typical of that described by Dikau et al. (1996) as a rock avalanche which has been constrained by a steep valley and formed a landslide lake.

On April 2 1999, Clanwilliam landslide occurred on a south facing slope above Clanwilliam Lake, approximately 13 km west of Revelstoke, B.C. The failed mass is composed of gneissic material, that in the case of Jure is meta-sandstones and Pelitic schist. The published data examination shows that no earthquake events were recorded prior to the Clanwilliam failure. The climatic record showed that pronounced freeze- thaw cycles occurred the day before and on the day of the failure. Only a significant amount of precipitation (20–25 mm/day) was recorded eleven days before the failure. On the other hand, a heavy rainfall was recorded two days before the Jure landslide. The Clanwilliam landslide area exhibits classical morphology with steep rock walls and a valley bottom (Fig. 16a). The Jure area exhibits similar topography and morphology (Fig. 16b), with steep rock slopes and narrow valley bottom formed by river erosion.

In case of Clanwilliam landslide, the preliminary kinematic analysis identified the potential slope failure mechanisms and was followed by limit equilibrium wedge analysis. The block theory analysis was undertaken to identify critical blocks and block shapes within the rockmass. The results of this study were used to perform a preliminary 3D-distinct element analysis that shows simple and complex wedge blocks appear to be a feasible failure mechanism for the Clanwilliam landslide (Grenon and Hadjigeorgiou 2003). It also emphasized that the orientations of discontinuities assigned to a joint set during the kinematic analysis can have a critical role on the stability of a rock slope.

Moreover, freeze–thaw cycles could have influenced the pore water pressure by obstructing some of the discontinuities with ice near the surface. Several workers have suggested such a phenomenon at a range of slope failure scales (Gardner 1983; Haeberli et al. 1997). In case of Jure, rainwater and surface water percolation through tension cracks and discontinuities is capable of increasing water pressure in networks of joints and tension cracks. The back analysis performed using various 2D and 3D analytical and numerical methods are useful in evaluating the role of the different discontinuity sets observed at the Clanwilliam landslide and Jure rock avalanche. Similar results and nature of the failure mechanism can be observed, which is a positive correlation. The Clanwilliam landslide is a progressive failure, where small movement accumulates along discontinuity and rock bridges are broken over a period of many years until a critical state is reached. As stated above, the current theory for the Jure avalanche is also a progressive failure due to high water pressure concentration around key blocks which was thrown outward when the hydrostatic pressure became greater than confining pressure.

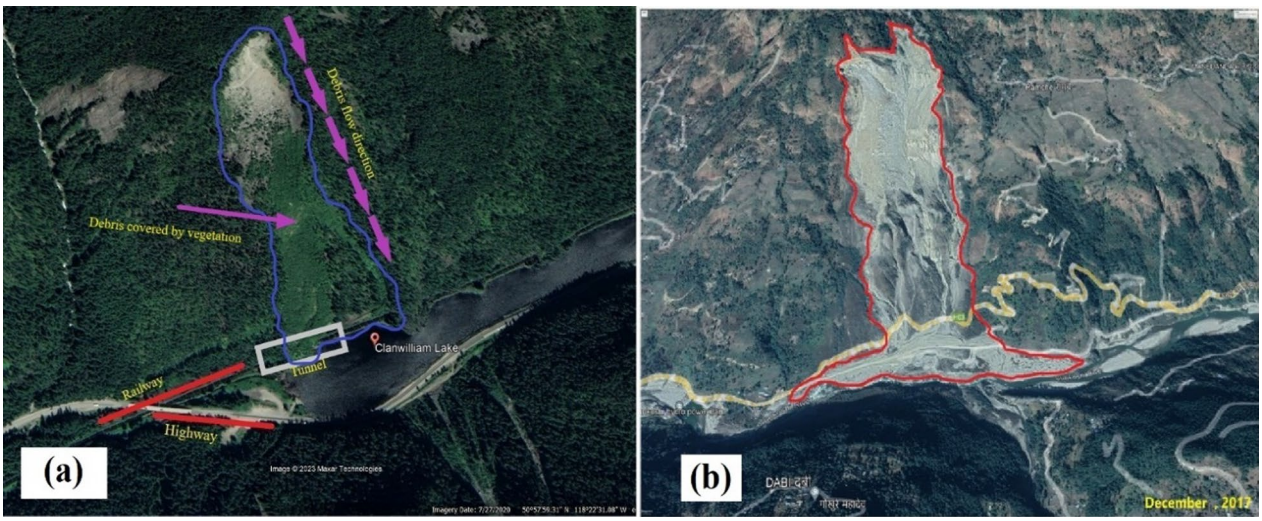

Fig. 16 Overview of the Clanwilliam landslide and Jure rock avalanches, **a** Clanwilliam landslide, **b** Jure rock avalanche (Google Earth)

Conclusion

The following conclusion can be drawn from the present study:

1. Pelitic schist, chlorotic schist and metasandstone are the dominant rock types observed in the study area. The Rock mass rating indicates metasandstone as a good rock mass and pelitic schist a fair rock mass. Additionally, geotechnical attributes like UCS, tensile strength, and friction angle of metasandstone are greater than that of schist.
2. Surface water from small streams percolated through the ground following open joints and tension crack over a period of time causing weathering/degradation of rockmass and creating a high pore-water pressure concentration in some area behind the upper cliff.
3. Heavy precipitation two days prior to the event increased the hydrostatic pressure that exceeded the static frictional threshold that caused blocks of schist to bulge due to its porous nature. Thus, the high-water table resulted in an explosion like fracturing of rocks and the expulsion of the block that supported the overlying mass.
4. Movement of the key block followed by planar sliding of wedges and foot failure appears to be a possible failure mechanism and propagates towards the crown after the main failure event happened.
5. No single slope stability analysis method can explain the failure mechanism of such large natural rock slopes. Various methods should be incorporated for better understanding of the behaviour and failure mechanism of rock slopes.
6. According to geometry the slope is kinematically stable, however water forces and slope geometry can cause a decrease in factor of safety. Therefore, similar analysis can be replicated for other critical areas for further stability analysis, owing to heavy rainfall for safe slope conditions. Moreover, water channel management around the slope is necessary to prevent future landslide reactivation.

Acknowledgements
SP & SD would like to thank the Central Department of Geology, Tribhuvan University, Nepal for providing the necessary assistance. AK would like to thank IOE-BHU for seed grant. AK would like to thank Rocscience, Canada for the analysis tool.

Author contributions
SP, SD, VHRP & VY conducted the field investigation, data exploration and analysis. PKS and AK wrote the MS and interpreted the data. All authors reviewed the manuscript.

Funding
Non-funded work.

Availability of data and materials
Obtain and available data is given in the same paper.

Declarations

Competing interests
All authors declare that they have no competing interests.

Received: 6 April 2023 Accepted: 25 October 2023
Published online: 29 October 2023

References

Achu AL, Joseph S, Aju CD et al (2021) Preliminary analysis of a catastrophic landslide event on 6 August 2020 at Pettimudi, Kerala State, India. Landslides 18:1459–1463. https://doi.org/10.1007/s10346-020-01598-x
Arnold M (2006) Natural disaster hotspots: Case studies. Disaster Risk Management No. 6 © Washington, DC: World Bank. http://hdl.handle.net/10986/7091
Auden JB (1937) The geology of the Himalaya in Garhwal, Part 4. Rec Geol Surv India 71:407–433 (with 3 plates, including a long cross-section on the scale of 1 inch = 2 miles)
Bhandary NP, Tiwari RC, Yatabe R, Paudel S (2018) SEM-based seismic slope stability and mitigation model for the jure landslide after the 7.8Mw 2015 Barpak-Gorkha, Nepal, Earthquake. In: Geotechnical earthquake engineering and soil dynamics V, pp 88–97. https://doi.org/10.1061/9780784481486.010
Bhandary NP, Yatabe R, Dahal RK, Hasegawa S, Inagaki H (2013) Areal distribution of large-scale landslides along highway corridors in central Nepal. Georisk Assess Manag Risk Eng Syst Geohazards 7(1):1–20. https://doi.org/10.1080/17499518.2012.743377
Bieniawski ZT (1973) Engineering classification of jointed rock masses. Civil Eng South Africa 15:335–343
Bieniawski ZT (1989) Engineering rock mass classifications. Wiley, New York, p 251
Bray S (2016) Slope failure along the Araniko highway from Jure to Tatopani. MSc thesis, University of Leeds, UK, p 54
Budhathoki R (2016) Cause and mechanism of 2014 Jure rock avalanche in Sindhupalchok district, Central Nepal. M.Sc. Thesis, Tribhuvan University, Nepal. p 71
Çelik M (2023) Investigating the performance of passageway corridor for ground reinforced embankments against rockfall. J Mt Sci 20:15–30. https://doi.org/10.1007/s11629-022-7559-3
Cui P, Zeng C, Lei Y (2015) Experimental analysis on the impact force of viscous debris flow. Earth Surf Proc Land 40(12):1644–1655. https://doi.org/10.1002/esp.3744
Dahal RK, Hasegawa S (2008) Representative rainfall thresholds for landslides in the Nepal Himalaya. Geomorphology 100(3–4):429–443. https://doi.org/10.1016/j.geomorph.2008.01.014
Dhital MR (2014) Causes and consequences of Seti glacial disaster and Jure rock avalanche in Nepal Himalaya. J Nepal Geol Soc 48(1):35–42
Dhital MR (2015) Geology of the Nepal Himalaya: regional perspective of the classical collided orogen. Springer, Cham, p 498
Dhungana G, Ghimire R, Poudel R, Kumal S (2023) Landslide susceptibility and risk analysis in Benighat Rural Municipality, Dhading. Nepal Nat Hazards Res 3(2):170–185. https://doi.org/10.1016/j.nhres.2023.03.006
Dikau R, Brunsden D, Schrott L, Ibsen ML (1996) Landslide recognition: identification, movement, and causes. Wiley, New York, p 274
Evans SG, Delaney KB, Hermanns RL, Strom A, Scarascia-Mugnozza G (2011) The formation and behaviour of natural and artificial rockslide dams; implications for engineering performance and hazard management. In: Evans S, Hermanns R, Strom A, Scarascia-mugnozza G (eds) Natural and artificial rockslide dams. Lecture notes in earth sciences, vol 133. Springer, Berlin, pp 1–75. https://doi.org/10.1007/978-3-642-04764-0_1
Gansser A (1964) Geology of the Himalayas. Interscience Publication, Wiley, London, p 289

Gardner J (1983) Rockfall frequency and distribution in the Highwood Pass Area. Can Rocky Mt Zeitschrift Für Geomorphologie 27(3):311–324
Grenon M, Hadjigeorgiou J (2003) Open slope stability using 3D joint networks. Rock Mech Rock Eng 36(3):183–208. https://doi.org/10.1007/s00603-002-0042-0Rock
Griffiths DV, Lane PA (2001) Slope stability analysis by finite elements. Géotechnique 51(7):653–654. https://doi.org/10.1680/geot.51.7.653.51390
Gutiérrez-Martín A, Herrada MÁ, Yenes JI, Castedo R (2019) Development and validation of the terrain stability model for assessing landslide instability during heavy rain infiltration. Nat Hazards Earth Syst Sci 19:721–736. https://doi.org/10.5194/nhess-19-721-2019
Haeberli W, Wegmann M, Muhll DV (1997) Slope stability problems related to glacier shrinkage and permafrost degradation in the Alps. Eclogae Geol Helv 90:407–414. https://doi.org/10.5169/seals-168172
Hencher S, Malone A (2008) Back analysis of landslides to allow the design of cost-effective mitigation measures
Hungr O, Evans S (2004) Entrainment of debris in rock avalanches: An analysis of a long run-out mechanism. Geol Soc Am Bull 116(9–10):1240–1252. https://doi.org/10.1130/B25362.1
Hungr O, Evans S, Bovis M, Hutchinson JN (2001) Review of the classification of landslides of the flow type. Environ Eng Geosci 7:221–238. https://doi.org/10.2113/gseegeosci.7.3.221
Hussain M, Stark T, Akhtar K (2010) Back-analysis procedure for landslides. In: Proceedings of the international conference on geotechnical engineering. Pakistan Geotechnical Engineering Society, Lahore, Pakistan, pp 159–166
Iqbal J, Dai F, Hong M, Tu X, Xie Q (2018) Failure Mechanism and Stability Analysis of an Active Landslide in the Xiangjiaba Reservoir Area. Southwest China J Earth Sci 29:646–661. https://doi.org/10.1007/s12583-017-0753-5
Jaboyedoff M, Leibundgut G, Penna I, Dahal RK, Sanjaya S, Karen S (2015a) Characterization of the Jure (Sindhupalchok, Nepal) Landslide by TLS and field investigations. Geophys Res Abstr 17:2015–11858
Jaboyedoff M, Leibundgut G, Penna I, Dahal RK, Sevkota S, Sudmeier K (2015) Characterization of the Jure (Sindhupalchok, Nepal) Landslide by TLS and field investigations. In: EGU General Assembly Conference Abstracts p 11858.
Kainthola A, Sharma V, Pandey VHR, Jayal T, Singh M, Srivastav A, Singh PK, Champati Ray PK, Singh TN (2021) Hill slope stability examination along Lower Tons valley, Garhwal Himalayas, India. Geomat Nat Haz Risk 12(1):900–921. https://doi.org/10.1080/19475705.2021.1906758
Kulatilake PHSW, Wang L, Tang H, Liang Y (2011) Evaluation of rock slope stability for Yujian River dam site by kinematic and block theory analyses. Comput Geotech 38:846–860. https://doi.org/10.1016/j.compgeo.2011.05.004
Lateltin O, Haemmig C, Raetzo H, Bonnard C (2005) Landslide risk management in Switzerland. Landslides 2:313–320. https://doi.org/10.1007/s10346-005-0018-8
Li MH, Sung RT, Dong JJ, Lee CT, Chen CC (2011) The formation and breaching of a short-lived landslide dam at Hsiaolin Village, Taiwan—Part II: simulation of debris flow with landslide dam breach. Eng Geol 123(1–2):60–71. https://doi.org/10.1016/j.enggeo.2011.05.002
Liu J, Hy Fu, Yb Z et al (2023) Effects of the probability of pulse-like ground motions on landslide susceptibility assessment in near-fault areas. J Mt Sci 20:31–48. https://doi.org/10.1007/s11629-022-7527-y
Lowe DR, Williams SN, Leigh H, Connort CB, Gemmell JB, Stoiber RE (1986) Lahars initiated by the 13 November 1985 eruption of Nevado del Ruiz, Colombia. Nature 324:51–53. https://doi.org/10.1038/324051a0
Mebrahtu TK, Heinze T, Wohnlich S, Alber M (2022) Slope stability analysis of deep-seated landslides using limit equilibrium and finite element methods in Debre Sina area, Ethiopia. Bull Eng Geol Env 81:403. https://doi.org/10.1007/s10064-022-02906-6
Ministry of Irrigation (MoI), Nepal government (2014) Report on Jure landslide, Mankha VDC, Sindhupalchowk district
Miyagi T, Yamashina S, Esaka F et al (2011) Massive landslide triggered by 2008 Iwate-Miyagi inland earthquake in the Aratozawa Dam area, Tohoku, Japan. Landslides 8:99–108. https://doi.org/10.1007/s10346-010-0226-8
Pandey VHR, Kainthola A, Sharma V, Srivastav A, Jayal T, Singh TN (2022) Deep learning models for large-scale slope instability examination in Western Uttarakhand. India Environ Earth Sci 81(20):487. https://doi.org/10.1007/s12665-022-10590-8
Panthee S, Singh PK, Kainthola A, Singh TN (2016) Control of rock joint parameters on deformation of tunnel opening. J Rock Mech Geotech Eng 8(4):489–498. https://doi.org/10.1016/j.jrmge.2016.03.003
Paul SK, Bartarya SK, Rautela P, Mahajan AK (2000) Catastrophic mass movement of 1998 monsoons at Malpa in Kali Valley, kumaun Himalaya (India). Geomorphology 35(3–4):169–180. https://doi.org/10.1016/S0169-555X(00)00032-5
Prakasam C, Aravinth R, Kanwar VS, Nagarajan B (2021) Comparative evaluation of various statistical models and its accuracy for landslide risk mapping: a case study on part of Himalayan Region, India. Slope Engineering In techOpen, India. https://doi.org/10.5772/intechopen.94347
Sartori M, Baillifard F, Jaboyedoff M, Rouiller JD (2003) Kinematics of the 1991 Randa rockslides (Valais, Switzerland). Nat Hazards Earth Syst Sci 3(5):423–433. https://doi.org/10.5194/nhess-3-423-2003
Shrestha BB, Nakagawa H (2016) Hazard assessment of the formation and failure of the Sunkoshi landslide dam in Nepal. Nat Hazards 82:2029–2049. https://doi.org/10.1007/s11069-016-2283-3
Stöcklin J, Bhattarai KD (1977) Geology of Kathmandu area and central Mahabharat Range, Nepal Himalaya. HMG/UNDP Mineral Exploration Project, Technical Report, 86 pp (with 15 maps), unpublished
Tien PV, Luong LH, Sassa K, Takara K, Sumit M, Nhan TT, Dang K, Duc DM (2021) Mechanisms and modeling of the catastrophic landslide dam at Jure Village, Nepal. J Geotech Geoenviron Eng 147(11):05021010. https://doi.org/10.1061/(ASCE)GT.1943-5606.0002637
Tien PV, Sassa K, Takara K et al (2018) Formation process of two massive dams following rainfall-induced deep-seated rapid landslide failures in the Kii Peninsula of Japan. Landslides 15:1761–1778. https://doi.org/10.1007/s10346-018-0988-y
Tiwari VN, Pandey VHR, Kainthola A, Singh PK, Singh KH, Singh TN (2020) Assessment of Karmi Landslide Zone, Bageshwar, Uttarakhand, India. J Geol Soc India 96:385–393. https://doi.org/10.1007/s12594-020-1567-0
Upreti BN (1999) An overview of the stratigraphy and tectonics of the Nepal Himalaya. J Asian Earth Sci 17:577–606. https://doi.org/10.1016/S1367-9120(99)00047-4
Varnes DJ (1978) Slope movement types and processes. Transportation Research Board Special Report, p 176. https://doi.org/10.53055/ICIMOD.240
Wang NF, He JX, Du XX et al (2023) Deformation and failure mechanism of Yanjiao rock slope influenced by rainfall and water level fluctuation of the Xiluodu hydropower station reservoir. J Mt Sci 20:1–14. https://doi.org/10.1007/s11629-022-7755-0
Wei ZL, Lü Q, Sun HY, Shang YQ (2019) Estimating the rainfall threshold of a deep-seated landslide by integrating models for predicting the groundwater level and stability analysis of the slope. Eng Geol 253:14–26. https://doi.org/10.1016/j.enggeo.2019.02.026
Wieczorek GF, Larsen MC, Eaton LS, Morgan BA, Blair JL (2001) Debris-flow and flooding hazards associated with the December 1999 storm in coastal Venezuela and strategies for mitigation. https://doi.org/10.3133/ofr01144
Xiao Z, Xu C, Huang Y, et al. (2023) Analysis of spatial distribution of landslides triggered by the Ms 6.8 Luding earthquake in China on September 5, 2022. Geoenvironmental Disasters 10:3 https://doi.org/10.1186/s40677-023-00233-w
Yagi H, Sato G, Sato HP, et al (2021) Slope Deformation caused Jure Landslide 2014 Along Sun Koshi in Lesser Nepal Himalaya and Effect of Gorkha Earthquake 2015. In: Vilimek V, wang F, Strom A, Sassa K, Bobrowsky PT (eds) understanding and reducing landslide disaster risk. WLF 2020. ICL Contribution to Landslide Disaster Risk Reduction. Springer, Cham, pp 65–72. https://doi.org/10.1007/978-3-030-60319-9_5
Yang B, Hou Jr, Zhou Zh et al (2023) Influence of different soil properties on the failure behavior of deposit slope under earthquake after rainfall. J Mt Sci 20:65–77. https://doi.org/10.1007/s11629-021-7243-z
Yin Y, Wang F, Sun P (2009) Landslide hazards triggered by the 2008 Wenchuan earthquake, Sichuan, China. Landslides 6:139–152. https://doi.org/10.1007/s10346-009-0148-5
Zhang Y, Shao JF, Xu WY et al (2014) Stability analysis of a large landslide in hydropower engineering. Nat Hazards 70:527–548. https://doi.org/10.1007/s11069-013-0826-4

Zhou JW, Xu WY, Yang XG (2010) The 28 October 1996 landslide and analysis of the stability of the current Hua-shiban slope at the Liang-jiaren Hydropower Station, Southwest China. Eng Geol 114:45–56
Zuo S, Zhao L, Deng D et al (2022) Back analysis of shear strength parameters for progressive landslides: case study of the Caifengyan landslide, China. Bull Eng Geol Env 81:19. https://doi.org/10.1007/s10064-021-02507-9

Publisher's Note